# A Study of Shared-Control With Bilateral Feedback for Obstacle Avoidance in Whole-Body Telelocomotion of a Wheeled Humanoid

DongHoon Baek, Yu-Chen Chang, and Joao Ramos

***Abstract*—Teleoperation has emerged as an alternative solution to fully-autonomous systems for achieving human-level capabilities on humanoids. Specifically, teleoperation with whole-body control is a promising hands-free strategy to command humanoids but requires more physical and mental demand. To mitigate this limitation, researchers have proposed shared-control methods incorporating robot decision-making to aid humans on low-level tasks, further reducing operation effort. However, shared-control methods for wheeled humanoid telelocomotion on a whole-body level has yet to be explored. In this work, we explore how whole-body bilateral feedback with haptics affects the performance of different shared-control methods for obstacle avoidance in diverse environments. A time-derivative Sigmoid function (TDSF) is implemented to generate more intuitive haptic feedback from obstacles. Comprehensive human experiments were conducted and the results concluded that bilateral feedback enhances the whole-body telelocomotion performance in unfamiliar environments but could reduce performance in familiar environments. Conveying the robot's intention through haptics showed further improvements since the operator can utilize the feedback for reactive short-distance planning and visual feedback for long-distance planning.**

***Index Terms*—Shared-control, whole-body telelocomotion, humanoid robot, bilateral feedback, obstacle avoidance.**

## I. Introduction

HUMANOID robots have been in the spotlight for a long time due to their promising potential to address problems in diverse scenarios from elderly care to disaster response [1], [2]. Despite the recent advancement, developing fully autonomous humanoid robots capable of achieving human-level adaptation in navigating harsh terrains and executing physical tasks is still extremely challenging.

In the face of the challenges, teleoperation emerged as an alternative solution where semi-autonomous humanoid robots are remotely controlled by humans [3]. By integrating human's ability to make adaptive decisions in complicated environments with robot's physical advantages in precision and repeatability, teleoperation has been widely used in many robotics applications, such as humanoids [4], surgical robots [5], mobile robots [6], and robot manipulators [7].

To teleoperate humanoids effectively, many human-machine interfaces (HMI) were developed to deliver human commands and receive feedback from the robot [4], [8]. However, direct teleoperation is challenging to employ when 1) the mapping between the robot's motion and the HMI is not intuitive to the operator, 2) the objects or obstacles locate outside of the camera's limited view or are partially occluded by the robot, 3) the visual feedback becomes mentally burdening in complicated environments. Such conditions are likely to increase the operator's effort and degrade performance while putting the robot in dangerous situations.

Shared-control [9] has emerged as a promising strategy to alleviate these limitations. This can be categorized into multiple strategies [10] with the overall goal to integrate decision-making from the robot to assist the human by detecting human intention, assigning control authority, and providing robot's feedback to the human [11]. The detection of human's intent and scenario-dependent control assignment can boost performance and make teleoperation more intuitive. Gottardi et al. [6] suggested a shared-control framework that utilized artificial potential fields (APF) to compensate the controller input by adding virtual repulsive and attractive points for better robot navigation. Wang et al. [12] proposed an adaptive servo-level shared-control scheme that combined tracking and obstacle avoidance controllers to generate shared-control output for assisting people with disability through a mobile robot. Song et al. [13] used human confidence level gains decided by distance to obstacle, operating speed, and operation time to decide the autonomous level in their shared-control framework for navigation. For providing feedback to the human on the robot's state and the environment, haptic feedback has been one of the effective approaches in shared-control applications since humans naturally use haptic communication during physical interactions [14]. Luo and Lin et al. [15] designed a shared-control framework with haptic feedback that detects human intention through EMG signals for obstacle avoidance. M Selvaggio et al. [16] proposed a task-prioritized shared-control method using haptic guidance

Manuscript received 21 June 2023; accepted 29 August 2023. Date of publication 11 September 2023; date of current version 19 September 2023. This letter was recommended for publication by Associate Editor G. Salvietti and Editor J.-H. Ryu upon evaluation of the reviewers' comments. This work was supported by the National Science Foundation under Grants IIS-2024775 and CMMI-2043339. *(DongHoon Baek and Yu-Chen Chang contributed equally to this work.) (Corresponding author: DongHoon Baek.)*

This work involved human subjects or animals in its research. Approval of all ethical and experimental procedures and protocols was granted by University of Illinois Urbana-Champaign.

DongHoon Baek is with the Department of Mechanical Science and Engineering, University of Illinois, Urbana-Champaign, Champaign, IL 61820 USA (e-mail: dbaek4@illinois.edu).

Yu-Chen Chang is with the Department of Electrical and Computer Engineering, University of Illinois, Urbana-Champaign, Champaign, IL 61820 USA (e-mail: yuchenc2@illinois.edu).

Joao Ramos is with the Department of Mechanical Science and Engineering, University of Illinois, Urbana-Champaign, Champaign, IL 61820 USA, and also with the Department of Electrical and Computer Engineering, University of Illinois, Urbana-Champaign, Champaign, IL 61820 USA (e-mail: jlramos@illinois.edu).

This letter has supplementary downloadable material available at https://doi.org/10.1109/LRA.2023.3313922, provided by the authors.

Digital Object Identifier 10.1109/LRA.2023.3313922

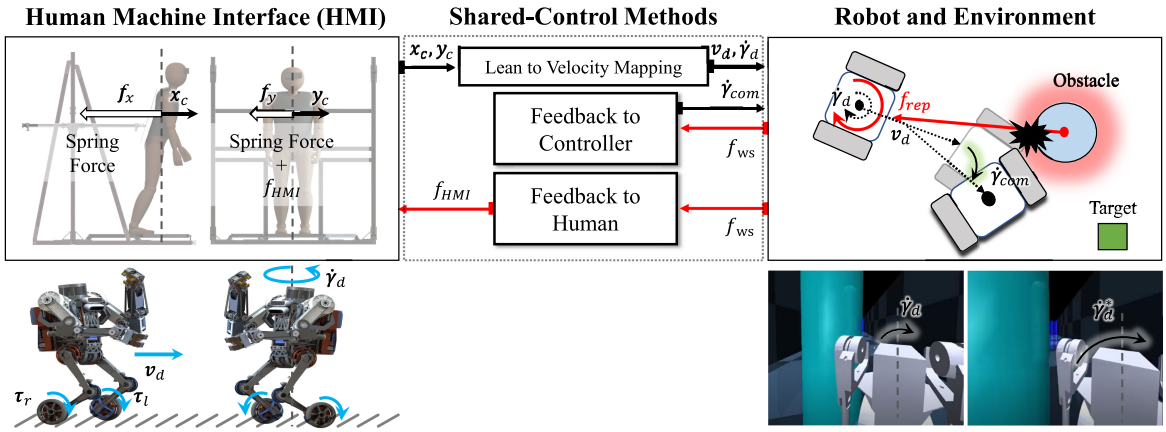


Fig. 1. Shared-control framework. The operator controls SATYRR through the whole-body HMI by changing the CoM. SATYRR moves forward and rotates when the operator leans in the sagittal and frontal planes, (respectively). Two kinds of force feedback, F-H and F-C, aid the operator in avoiding collision by providing haptic feedback $f_x$ and $f_y$ ($f_{HMI}$ plus *spring force*) to the user and updating the velocity command, respectively. The obstacle repulsive force is calculated based on (1), (2), and (3).

to inform the operator on kinematic constraints of a redundant manipulator. Abi-Farraj et al. [17] utilized the haptic feedback to generate demonstrated trajectory distribution to decide the level of autonomy.

However, *no prior work has explored the effectiveness of providing haptic force feedback and autonomous controller through a whole-body HMI in a shared-control framework.* Such HMI with whole-body control and feedback allows hands-free telelocomotion, a subcategory of teleoperation where the operator remotely control the legged robot's locomotion [18]. This allows the operator to navigate and perform manipulation tasks simultaneously on a humanoid robot for more dynamic motions [1] but requires more mental and physical effort compared to performing the tasks sequentially. Incorporating shared-control strategies could reduce the telelocomotion difficulty for a whole-body HMI. With haptic force being a popular method for providing feedback to the human, the questions then become: 1) Could incorporating haptic feedback in a shared-control framework reduce the effort for obstacle avoidance with whole-body telelocomotion on a humanoid robot? 2) What level of autonomy and what feedback methods would humans prefer in what kind of environments?

In this work, we explore and compare the performance of multiple shared-control feedback approaches with bilateral haptic force for humanoid robot obstacle avoidance through whole-body telelocomotion. To the best of our knowledge, this is the first time to explore and apply the shared-control framework in whole-body level teleoperation to control a humanoid robot. Our main contributions are highlighted as follows: 1) a novel whole-body level shared-control framework with bilateral force feedback; 2) integration of a wheeled humanoid robot SATYRR in simulation, a whole-body HMI, and virtual reality (VR) devices; 3) extensive human experiments by comparing the performance and user satisfaction of four different shared-control feedback methods in five static and dynamic maps to explore the optimal tele-operation method for each situation.

## II. Method and Materials

The proposed whole-body level shared-control framework consists of three different components: 1. *default spring force* to aid a human by encouraging the user to tilt the body more to easily control the HMI. 2. *Feedback to human* enabling a person to feel physical force 3. *Feedback to controller* renovating the reference velocity tracked by the autonomous controller. These components are selectively leveraged to observe the influence of each factor in the experimental section.

### A. Wheeled Humanoid Robot and Human-Machine Interface

To evaluate different bilateral feedback methods in our shared-control framework, a wheeled humanoid robot SATYRR [1] and a whole-body HMI [8] were utilized as described in Fig. 1. SATYRR is a wheeled bipedal robot consisting of one torso, two three degree-of-freedom (3DOF) arms, two legs with knee and ankle joints, and two wheels for traversal. As regards to the whole-body HMI, two backdrivable linear sensor and actuators (LISA) were used to detect the operator's center of mass (CoM) while providing haptic force to the person's torso.

### B. Whole-Body Level Shared-Control Framework Using Bilateral Feedback

*1) Controller Design and Basic Teleoperation Law:* The overview of our shared-control framework is shown in Fig. 1. The operator's CoM displacement along the $x$-axis and $y$-axis is mapped to the forward velocity $v_{\mathrm{d}}$ and the angular velocity $\dot{\gamma}_{\mathrm{d}}$ around the vertical axis of the robot, respectively. Both of the desired velocities are fed into a Linear Quadratic Regulator (LQR) controller for balancing and a PD controller for turning, resulting with robot's wheel torques ($\tau_{\mathrm{r}}$ and $\tau_{\mathrm{l}}$). We adopted a velocity mapping strategy [1] that uses different slopes and a dead-band to ensure any undesired small displacement in the operator's CoM does not result in high frequency movement for the robot. The wheeled inverted pendulum (WIP) model is utilized to stabilize the robot.

*2) Obstacle Repulsive Force From Time-Derivative Sigmoid-Function:* To improve the operator's obstacle avoidance capability during telelocomotion, we generated repulsive feedback force for each obstacle to guide the robot away from potential collisions. Such repulsive force generated from an APF is commonly used in shared-control frameworks due to its low-computational cost [15]. Despite the APF's benefits, the force generated has several drawbacks when applied as feedback to

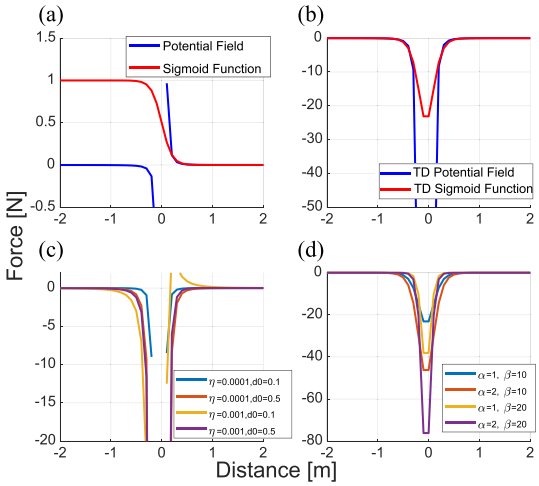


Fig. 2. Comparison of force profile. All figures assume the same constant velocity $\frac{dp}{dt}$. (a) and (b) indicate the force profiles for the time-derivative (TD) of APF and TDSF, respectively. (c) and (d) represent the resulting force profile of TD APF and TDSF respectively with various parameter values.

the operator's whole-body. Based on our empirical evidence, the operators felt uncomfortable being pushed or pulled by the obstacle repulsive force applied in the $x$-axis since they have less control of their balance in the sagittal plane while standing. The operators also felt discomfort from the constant feedback force generated from going around or moving at slower speed close to obstacles, considering that the magnitude of the APF force is decided only by the Euclidean distances between the robot and the obstacles. Moreover, tuning the desired force profile of the APF is not intuitive since both of its hyperparameters (see [19]) are coupled with the slopes of the force curves and activation distance as shown in Fig. 2.

In order to generate a more intuitive feedback force that also considers the relative velocities between the robot and the obstacles, we suggest to use the time-derivative of a Sigmoid function (TDSF) in place of the APF:

$$f_{\text{rep}}(p)=\begin{cases}\frac{d}{dt}F_{\text{rep}}(p)=\beta\frac{dF_{\text{rep}}(p)}{dp}\frac{dp}{dt}, & \text{if } p\le p_0 \text{and } \frac{dF_{\text{rep}}(p)}{dp}>0\\ 0, & \text{otherwise}\end{cases} \tag{1}$$

$$F_{\text{rep}}(p)=\frac{\alpha}{1+e^{\beta(-p)}} \tag{2}$$

where $p$ is the distance to each obstacle, $p_0$ is the force activation distance, $\alpha$ is the force magnitude gain, and $\beta$ represents the gain for changing the slopes of the force curves. Note that the TDSF can be replaced by other functions, such as an arctangent, that are similarly shaped for the benefits described as follows. As shown in Fig. 2, the TDSF generates less aggressive force compared to the APF while the activation distance and the slopes of the force curve $\frac{dF_{\text{rep}}(p)}{dp}$ are easier to tune with $\alpha$ decoupled from the activation distance. The time-derivative term $\frac{dp}{dt}$ denotes that more force is applied when the relative velocity between the robot and the obstacle is large while no force is generated at static or constant relative velocity. Moreover, the derivative term $\frac{dF_{\text{rep}}(p)}{dp}$ is zero if the robot stays equidistant from the obstacle, generating no feedback force when the robot is not approaching potential collision. When $\frac{dF_{\text{rep}}(p)}{dp}$ is non-positive, $f_{\text{rep}}(p)$ is set to zero since the robot is distancing from the obstacle. The weighted sum of obstacle repulsive force calculated by the sum of the forces generated from each obstacle and wall $f_{\text{ws}}$ is:

$$f_{\text{ws}}(\boldsymbol{p},g(\boldsymbol{\theta}))=-w_1\sum_{m=1}^{M}f_{\text{rep}}(p_{\text{m}})g(\theta_{\text{m}})-w_2\sum_{n=1}^{N}f_{\text{rep}}(p_{\text{n}})g(\theta_{\text{n}}) \tag{3}$$

where $\boldsymbol{p}$ is the vector set of distance $p$ ($p_i\in\boldsymbol{p}$). Symbols $w_1$ and $w_2$ are the weights of the force from the obstacles and the walls while $M$ and $N$ denote the number of obstacles and walls, respectively. The function $g(\theta)$ ($\theta_i\in\boldsymbol{\theta}$) takes in the angle between the obstacle and the robot's $x$-axis in the body frame and is defined with $g(\theta)=\text{atan2}(\vec{or}^{\,\text{i}}_{\text{y}},\vec{or}^{\,\text{i}}_{\text{x}})$, where symbols $\vec{or}^{\,\text{i}}_{\text{x}}$ and $\vec{or}^{\,\text{i}}_{\text{y}}$ represent the vectors from the robot to each obstacle $i$ in the body frame's x-axis and y-axis. This allows the function $f_{ws}$ to be aimed at generating a force in the direction of rotation.

*3) Feedback to Controller With Obstacle Repulsive Force:* One intuitive way for updating the controller command input to consider obstacle avoidance is by adding the obstacle repulsive force $\dot{\gamma}_{\text{com}}$ to the operator's commanded velocity $\dot{\gamma}_{\text{d}}$ [6], resulting with the updated angular velocity command $\dot{\gamma}^*_{\text{d}}$:

$$\dot{\gamma}^*_{\text{d}}=\lambda\dot{\gamma}_{\text{d}}+\dot{\gamma}_{\text{com}}=\lambda\dot{\gamma}_{\text{d}}+f_{\text{ws}}(\boldsymbol{p},g(\boldsymbol{\theta})) \tag{4}$$

where $\lambda$ is parameter of sensitivity and $g(\theta)$ represents the rotation angle of the yaw controller. Only the yaw velocity command is compensated based on an important insight from experiments that the operators dislike velocity modification in the $x$-axis.

*4) Haptic Feedback to Human With Obstacle Repulsive Force:* The haptic feedback ($f_x$ and $f_y$) provided to the operator is calculated by the sum of the force $f_{\text{ws}}(\boldsymbol{p},g(\boldsymbol{\theta}))$ with $g(\theta)=\sin(\text{atan2}(\vec{or}^{\,\text{i}}_{\text{y}},\vec{or}^{\,\text{i}}_{\text{x}}))$ and a *spring force* that helps maintain the neutral stance position:

$$f_{\text{x}}=-k_{\text{x}}(x_{\text{H}}-x_{\text{H}_0}) \tag{5}$$

$$f_{\text{y}}=-k_{\text{y}}(y_{\text{H}}-y_{\text{H}_0})-\mu f_{\text{ws}}(\boldsymbol{p},g(\boldsymbol{\theta})) \tag{6}$$

where $k_{\text{x}}$ and $k_{\text{y}}$ are the spring constants. Symbol $\mu$ represents the customizable force feedback gain. Symbols $x_{\text{H}}$ and $y_{\text{H}}$ are the operator's CoM position while $x_{\text{H}_0}$ and $y_{\text{H}_0}$ are the calibrated neutral CoM position in the x-axis and y-axis. Two LISAs equally contribute to generating the forces $f_{\text{x}}$ and $f_{\text{y}}$ in the transverse plane.

## III. Experiment

To exhaustively compare the effectiveness of the shared-control methods under diverse conditions, we conducted human experiments with static and dynamic obstacle maps under different brightness conditions and feedback cases.

### A. Participants

Nine subjects for unknown map and ten subjects for known map were recruited to complete the experiments. All subjects (both female and male) were within the age range of 22-34. The experiments were approved and conducted in compliance with the requirements from the Internal Review Board (IRB) of UIUC.

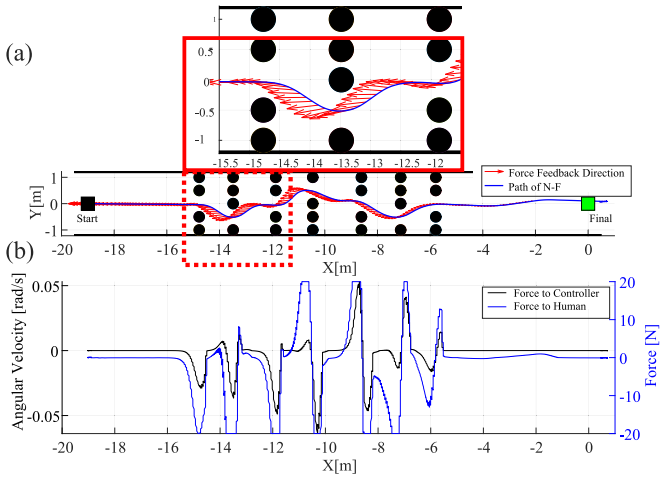


Fig. 3. Robot trajectory and force feedback. (a) Blue line is the path of No Feedback case (N-F) and red arrow shows the force direction applied to the robot. For example, the arrow below the blue line indicates the force to further rotate the robot clockwise. (b) Graph shows how force feedback is applied to the controller and human.

### B. Hardware and Simulation Experiment Setup

To accurately calculate the feedback force for each obstacle and wall in the maps, we integrated a SATYRR model in the MuJoCo physics simulation such that the robot can obtain the global positions of all obstacles within its force feedback activation distance. In all experiments, the operators were equipped with a VR headset (VIVE Pro Eye, HTC, Taiwan) that provided the view of a virtual camera attached to the robot as shown in Fig. 5. To reduce possible nausea from VR based on empirical evidence, the virtual camera was attached above and behind the robot such that the operator can see the robot's shoulder at all times, which is also a feasible configuration for the physical robot. Each participant completed five maps, with four feedback scenarios per map and five trials per scenario, totaling 1,000 trials. Each trial lasted between 40 seconds to two minutes. To avoid fatigue and biased results, participants had enough rest time based on individual preference and feedback scenarios were randomized for each map. A low pass filter was implemented for the camera's yaw that tracks the robot's yaw, mimicking a camera stabilizer that eliminates high frequency movement. The User Datagram Protocol (UDP) was used to communicate between the HMI and the MuJoCo simulation.

### C. Five Map Cases

The maps were designed based on our hypothesis that the operators will be less dependent on the robot's assistance in known environments where the optimal paths do not deviate while more reliant on the robot's decision making and the additional repulsive force feedback in unknown or mentally taxing environments. Concretely, two known maps have unvarying obstacle locations and velocities that were familiar to the operators, while three unknown maps involve randomized obstacle locations and velocities with different brightness configurations. The details of each map can be seen in Fig. 4 .

*1) Two Known Maps:* The experiments conducted on the two known maps explored the influence of bilateral feedback in environments familiar to the operator where the locations and velocities of all obstacles were predetermined. As shown in

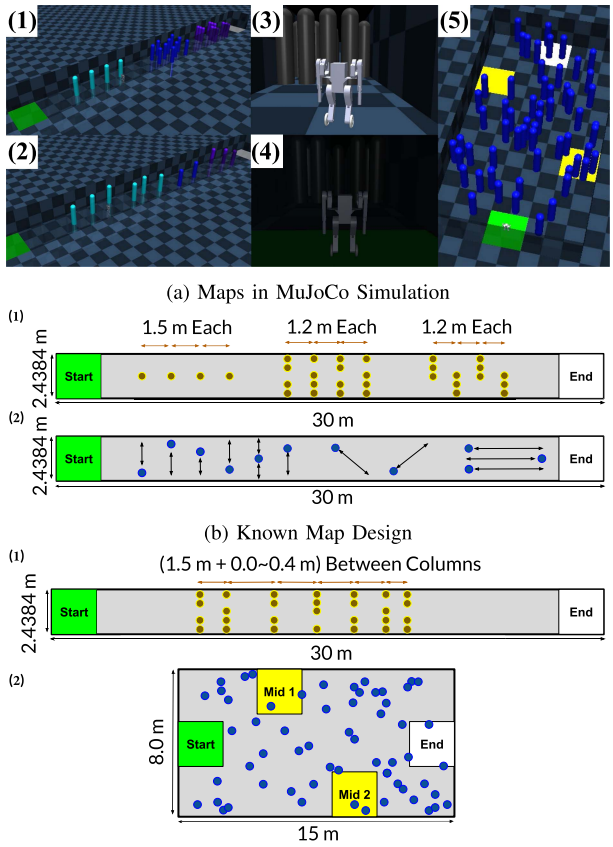


Fig. 4. Map design. (a.1) Known static map, (a.2) Known dynamic map, (a.3) Unknown bright static map, (a.4) Unknown dark static map, (a.5) Unknown dynamic map, (b.1) Static map, (b.2) Dynamic map, (c.1) Bright and dark static maps, and (c.2) Dynamic map.

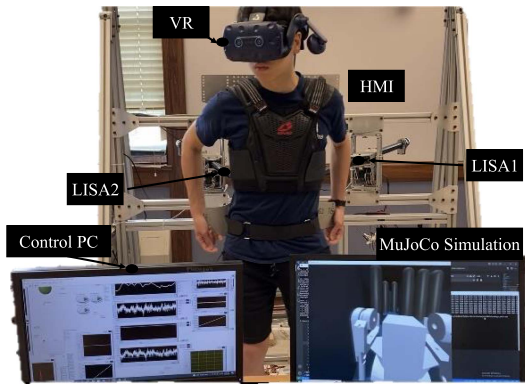


Fig. 5. Experiment setup.

Fig. 4, the experiments were conducted in two maps, one with static obstacles and one with dynamic obstacles. All obstacles have the same size and cylindrical shape, modeled from a human of 1.7 m with 0.2 m radius. In the static map, the operator has to pass the first four obstacles through a S-shaped route. The velocities of the dynamic obstacles are predetermined between 0.6 m/s to 0.9 m/s with fixed initial locations.

*2) Three Unknown Maps:* The experiments conducted in the three unknown maps were designed to evaluate the effect of bilateral feedback on performance in unfamiliar and complex

environments. The initial locations and velocities of the obstacles in the unknown static and dynamic maps were randomized in every experiment to prevent the subjects from learning the optimal paths. In the static map as shown in Fig. 4, the distance between the columns of obstacles and the removed obstacle in each column are randomized for varied turning and acceleration control. In addition to the regular bright static map, we designed a dark static map that has 10% brightness of the bright static map to examine sub-optimal visual feedback and its effect on the bilateral feedback usage. The dynamic map has 60 obstacles with two randomized required mid-points that appear close to either the top or bottom walls. In total, three unknown maps (static bright, static dark, and dynamic) were designed.

### D. Shared-Control Feedback Cases

Four shared-control feedback cases were tested on all five maps. The *default spring force* is applied to all feedback cases:

1) **No Feedback (N-F)**: basic telelocomotion without using any obstacle repulsive force. This is the method applied in the previous work [1].
2) **Feedback to Human (F-H)**: the obstacle repulsive force is applied as haptic feedback $f_{\text{HMI}}$ to the operator's torso.
3) **Feedback to Controller (F-C)**: the obstacle repulsive force modifies the controller's reference angular velocity $\dot{\gamma}_{\text{d}}$ so the robot automatically adjusts its trajectory.
4) **Mixed Feedback (M-F)**: a combination of F-H and F-C allows the operator to feel the haptic force feedback from F-H while F-C autonomously adjusts the robot's trajectory simultaneously. The force feedback activation distance for F-H is 25% further than F-C to prevent the operator from feeling the haptic feedback lagging behind the automatic compensated trajectory.

### E. Evaluation Procedure and Metrics

All subjects had sufficient practice to acclimate themselves to the VR headset, the dynamics of SATYRR, the HMI, and the tasks prior to the experiments. Moreover, the gain $\mu$ from (6). was tuned based on each subject's preference for the haptic force feedback strength.

To evaluate the performance of the cases carefully, we adopted the following evaluation metrics:

1) **Completion Time (C-T):** C-T represents the time measured when the operator finishes the task. The timer starts when the operator sees the virtual map and ends when the robot enters the white end zone or it crashes. A smaller number indicates a faster completion of the tasks.
2) **Collision Number (C-N):** C-N represents the total number of collisions per case divided by the number of trials per case. A smaller number indicates fewer collisions with obstacles.
3) **Completed Distance (C-D):** Since all maps have starting points and destinations in straight lines in the x-coordinate, C-D is the traversed distance divided by the distance from the start to the destination in the x-coordinate. A larger number indicates a higher completion percentage of the map.
4) **Success Rate (S-R):** S-R is the number of successfully completed trials divided by the total number of trials. A trial is successful if the robot moves from the starting location to the specified ending region in the maps. A trial is unsuccessful if the robot crashes into obstacles and cannot balance itself, subsequently crashing into the ground. Note that not all collisions result in a crash. A number closer to one indicates a higher success rate, considered as the most important metric.
5) **NASA-TLX and Interviews:** Workload and user satisfaction were assessed through the NASA Task Load Index (TLX) [20]. Interviews were conducted after all experiments to obtain qualitative feedback for each shared-control feedback case. The interview questions are included in the supporting materials.

## IV. Results and Discussion

To compare the effectiveness of different feedback cases in the five different maps, the following sections are separated into two analyses, one for the known maps and one for the unknown maps.

### A. Quantitative Results From the Known Map Experiments

*1) Known Static Map:* In most evaluation metrics, F-C and N-F tended to show better performance than others in the known static map (see Table I). For the individual subjects' best cases, more than half of the subjects performed the best with F-C. Since the controller automatically corrected the subjects' turning mistakes, the subjects could focus on deciding the overall long-term path and rely on the robot to make small adjustments for a safer path. Nevertheless, the subjects did not know the robot's intention prior to the automatic turns and had to predict the compensated trajectory based on the obstacle locations from visual feedback. After the subjects learned the best paths and strategies to complete the tasks, the haptic feedback that physically resisted the subjects' desired motions induced more mental and physical effort that degraded the performance (See Fig. 6).

*2) Known Dynamic Map:* Unlike the results in static map, using an autonomous controller (e.g., F-C and M-F) showed worse performance than N-F and F-H in the dynamic map overall (see Table I). For the individual subjects' best cases, N-F also outperformed other methods for more than half of the participants. Once the subjects got familiar with the map and discovered the optimal path, controlling the robot's forward motion and timing the moving obstacles became the key challenge. To overcome this, the subjects needed full control of the robot to perform more dynamic and responsive motions, so any additional controller compensation became a disturbance and added uncertainty. Moreover, the visual feedback was sufficient for predicting the obstacles' trajectories since the obstacle locations and velocities were known to the subject, so F-C which required mental effort to process was detrimental to performance.

### B. Qualitative Results From the Known Map Experiments

In both the static and dynamic maps, most subjects preferred N-F and reported the least frustration and physical demand as well as the best perceived performance through the NASA TLX (see Fig. 6). In the case of the performance index, the p-value was less than 0.01, and N-F was evaluated to have significantly better performance than other methods. F-C showed slightly less mental demand compared to N-F since the subjects could rely

TABLE I

AVERAGE AND INDIVIDUAL RESULTS FOR EACH METHODS IN THE KNOWN MAPS. MEAN AND STANDARD DEVIATION ARE CALCULATED BASED ON THE AVERAGE PERFORMANCE OF EACH PARTICIPANTS (MEAN: **M**, STANDARD DEVIATION: **S**). INDIVIDUAL RESULT REPRESENTS THE METHOD WITH THE HIGHEST NUMBER OF GOOD PERFORMERS IN THE RESULT OF EACH SUBJECT

| | | **Static Map** | | | | | | | | **Dynamic Map** | | | | | | | |
|---|---|---|---|---|---|---|---|---|---|---|---|---|---|---|---|---|---|
| | | **C-T[s] (m, s)** | | **C-N[%] (m, s)** | | **C-D[%] (m, s)** | | **S-R[%] (m, s)** | | **C-T[s] (m, s)** | | **C-N[%] (m, s)** | | **C-D[%] (m, s)** | | **S-R[%] (m, s)** | |
| **Method** | **N-F** | **87.15** | 28.5 | 0.87 | 0.77 | 0.83 | 0.13 | 0.62 | 0.27 | **75.36** | 11.42 | **0.42** | 0.37 | 0.78 | 0.17 | 0.62 | 0.29 |
| | **W F-H** | 91.1 | 26.57 | 0.78 | 0.74 | 0.86 | 0.14 | 0.67 | 0.26 | 76.64 | 10.04 | 0.44 | 0.46 | **0.88** | 0.11 | **0.69** | 0.23 |
| | **W F-C** | 92.99 | 32.10 | 0.53 | 0.55 | **0.88** | 0.13 | **0.73** | 0.30 | 81.09 | 20.77 | 0.62 | 0.38 | 0.77 | 0.16 | 0.58 | 0.29 |
| | **M-F** | 98.77 | 42.37 | **0.51** | 0.39 | 0.83 | 0.16 | 0.64 | 0.31 | 79.03 | 15.46 | 0.64 | 0.47 | 0.78 | 0.17 | 0.56 | 0.30 |
| **Individual Result** | | **N-F** | | **F-C** | | **F-C** | | **F-C** | | **N-F** | | **N-F** | | **F-H** | | **F-H** | |

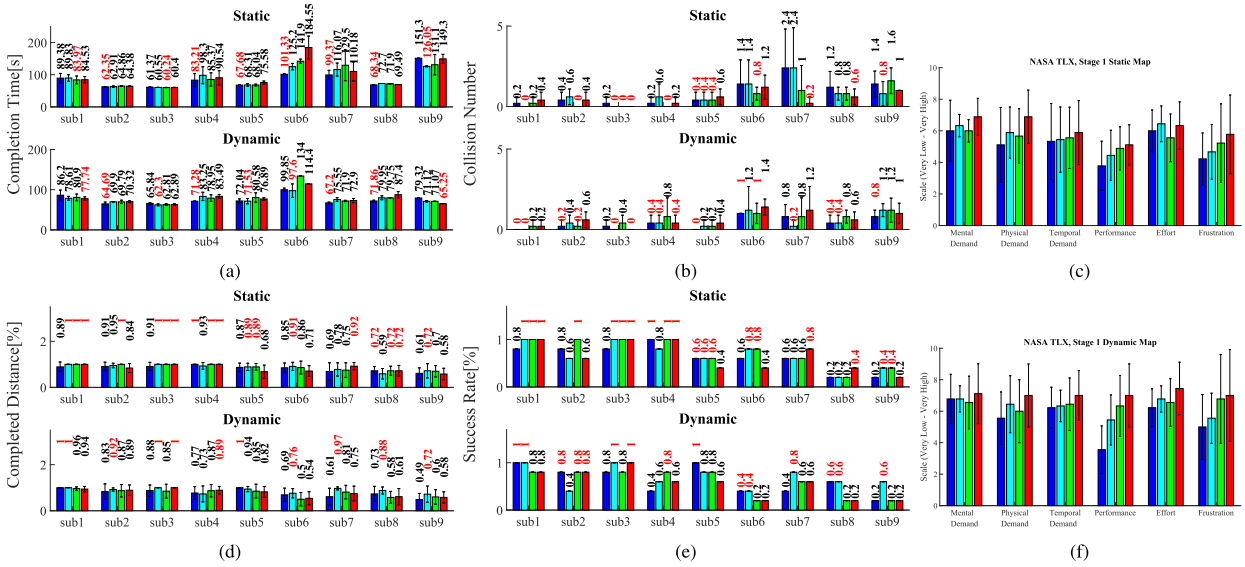


Fig. 6. Each subject's results and NASA TLX summary for the known map. (a), (b), (d), and (e) indicate the mean and standard deviation of the nine subjects' performance in the static and dynamic maps with five trials per method. The numerical values above the bars represent the mean values with the red texts representing the best performing cases. (c) and (f) show the NASA TLX result average in the static and dynamic maps, respectively. (BLUE: N-F, CYAN: F-H, GREEN: F-C, RED: M-F).

TABLE II

AVERAGE AND INDIVIDUAL RESULTS FOR EACH METHOD IN THE UNKNOWN MAP EXPERIMENTS MEAN AND STANDARD DEVIATION ARE CALCULATED BASED ON THE AVERAGE PERFORMANCE OF EACH PARTICIPANT (MEAN: **M**, STANDARD DEVIATION: **S**). THE INDIVIDUAL RESULT REPRESENTS THE METHOD WITH THE HIGHEST NUMBER OF GOOD PERFORMERS IN THE RESULT OF EACH SUBJECT

| | | **Static Dark Map** | | | | | | | | **Static Bright Map** | | | | | | | | **Dynamic Map** | | | | | | | |
|---|---|---|---|---|---|---|---|---|---|---|---|---|---|---|---|---|---|---|---|---|---|---|---|---|---|
| | | **C-T[s] (m, s)** | | **C-N[%] (m, s)** | | **C-D[%] (m, s)** | | **S-R[%] (m, s)** | | **C-T[s] (m, s)** | | **C-N[%] (m, s)** | | **C-D[%] (m, s)** | | **S-R[%] (m, s)** | | **C-T[s] (m, s)** | | **C-N (m, s)** | | **C-D[%] (m, s)** | | **S-R[%] (m, s)** | |
| **Method** | **N-F** | 47.87 | 8.64 | 0.76 | 0.39 | 0.82 | 0.12 | 0.64 | 0.21 | 45.88 | 8.84 | 0.60 | 0.43 | 0.85 | 0.20 | 0.72 | 0.25 | 42.70 | 7.74 | 0.56 | 0.34 | 0.80 | 0.17 | 0.22 | 0.19 |
| | **F-H** | 48.16 | 9.09 | 0.55 | 0.52 | 0.89 | 0.12 | **0.80** | 0.23 | 46.71 | 9.92 | 0.70 | 0.61 | 0.84 | 0.13 | 0.70 | 0.27 | **42.48** | 7.43 | 0.60 | 0.28 | 0.78 | 0.14 | 0.22 | 0.15 |
| | **F-C** | 47.78 | 8.46 | 0.42 | 0.26 | 0.86 | 0.12 | 0.68 | 0.27 | 45.32 | 5.98 | **0.50** | 0.27 | 0.86 | 0.08 | 0.68 | 0.19 | 45.49 | 8.81 | 0.56 | 0.31 | **0.81** | 0.17 | 0.22 | 0.17 |
| | **M-F** | **46.47** | 7.96 | **0.36** | 0.42 | **0.92** | 0.09 | **0.80** | 0.27 | **44.25** | 6.56 | 0.54 | 0.37 | **0.90** | 0.09 | **0.78** | 0.18 | 43.35 | 9.29 | **0.52** | 0.34 | **0.81** | 0.14 | **0.28** | 0.24 |
| **Individual Result** | | **M-F** | | **M-F** | | **M-F** | | **M-F** | | **N-F, F-C, M-F** | | **F-C** | | **M-F** | | **M-F** | | **N-F** | | **F-C** | | **F-C** | | **F-H, M-F** | |

on the robot to make small adjustments for obstacle avoidance. However, F-C sometimes generated unexpected robot trajectory especially when the obstacles were moving, resulting in more frustration and worse perceived performance. With the M-F, the subjects had to put in more mental and physical effort since the haptic force and the compensated controller caused disturbance and uncertainty to the control in a known environment, which led to the most effort and frustration with the worst perceived performance.

### C. Quantitative Results From the Unknown Map Experiments

*1) Unknown Static Dark Map:* The advantages of using bilateral feedback are revealed in unfamiliar environments. In the unknown static dark map, M-F outperformed the other methods in all evaluation metrics (see Table II) and likewise in the results for each participant shown in Fig. 7. Specifically, in Hypothesis testing with statistical analysis, $p$-value of (N-F, C-F) and (N-F, M-F) regarding the collision number and (N-F, M-F)

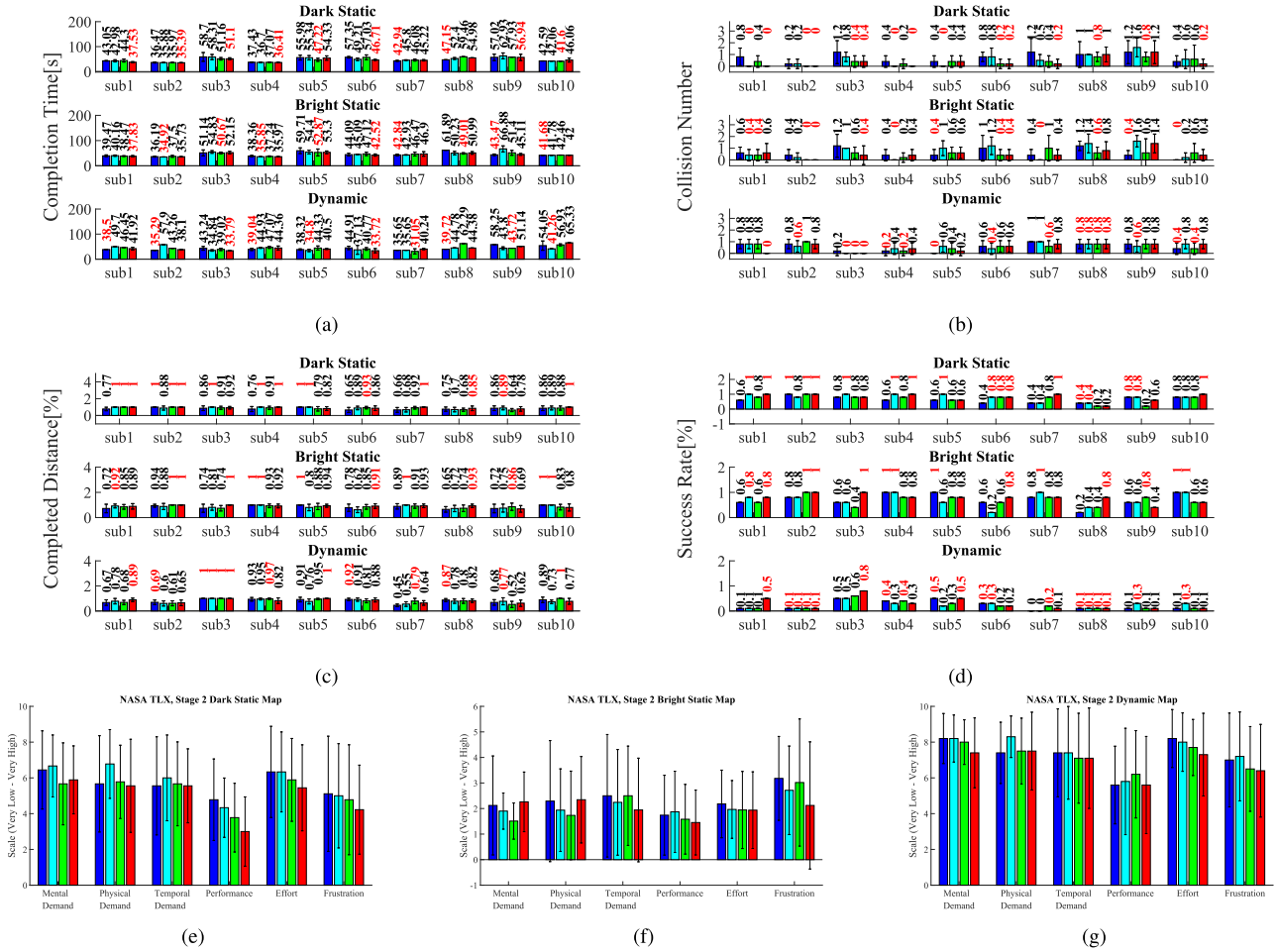


Fig. 7. Result of each subject for each method in the unknown map experiments. (a)–(d) represent the mean and standard deviation of each subject's static maps (bright and dark) and dynamic map performance for the four feedback methods. The numerical values above the bars represent the mean values with the red texts representing the best performing cases. (e)–(g) show the NASA TLX result in the static maps (bright,dark) and dynamic map. (Blue: N-F, CYAN: F-H, GREEN: F-C, RED: M-F).

regarding the completed distance are less than 0.05, showing the significance ($p$-value is $0.016, 0.019, 0.019$ in order). Due to the reduced visual feedback and the randomized paths, the operators had to learn and rely more on the compensated controller and the haptic feedback combination. This trend is further demonstrated with F-H and F-C where both feedback cases showed better performance than N-F, suggesting that more feedback is consistently more useful in unfamiliar environments with reduced visual information. The subjects could intuitively understand the robot's automatic turning intention since the activation distance for F-H in M-F is further than F-C as described in the experiment section. The subjects also had the final decision power over the automatic turns by fighting against F-H that reflected F-C.

*2) Unknown Static Bright Map:* In the unknown static bright map, M-F showed its strength in both the aggregated results and individual outcomes (see Table II and Fig. 7). The F-C and M-F showed less C-N compared to others, indicating that the autonomous controller is helpful for avoiding collisions in the unknown static bright map. Note that the C-N is higher in the bright static map than the dark static map since the subjects were more cautious and moved slower in the dark map as shown through C-T.

*3) Unknown Dynamic Map:* In this complex environment where numerous obstacles moved with random velocities, M-F showed its strengths compared to other methods (see Table II). This indicates that shared-control is advantageous in complicated and visual sensory overloading environments where the operator has to make many predictions and decisions. M-F outperformed F-H and F-C since the subjects could rely on F-C for automatic turns while using F-H to understand the robot's intention quickly in the dynamic environment. The automatic turns in F-C and M-F saved the subjects from many close collision encounters, demonstrated with less C-N and higher C-D. Although N-F has lower C-T for the individual results, the difference is negligible (only one person).

### *D. Qualitative Results From the Unknown Map Experiments*

The NASA TLX results shown in Fig. 7 denote that the subjects preferred shared-control methods over N-F in all unknown maps. Regarding performance metrics, the p-value was found to be below 0.05. This indicated that M-F significantly outperformed both N-F and F-H. In our interviews, the majority of the subjects also indicated that they preferred M-F over other feedback cases. We note that this shows a marked difference from the result pattern in the known map. Most subjects

mentioned that they made use of the visual feedback for path planning in the longer distance while using the automatic turns and force feedback to avoid obstacles in the shorter distance. F-H was useful for alerting about potential collisions, but manual obstacle avoidance was physically demanding. Similarly, while F-C corrected many user errors effectively, its automatic turns could sometimes overcompensate or be unpredictable, leading to increased physical effort.

### *E. Limitations*

Although bilateral feedback in our shared-control framework showed better performance in various conditions, our research has several limitations to be further improved. First, most experimental results were not very statistically significant. Nonetheless, our results provide insight into humanoid control strategies using whole-body teleoperation by showing which feedback methods are useful under which circumstances. Second, the operators controlled and received force feedback from the robot yaw through the less intuitive frontal plane motion due to the HMI configurations. Matching the robot's yaw with the human's yaw motion could further improve the performance of the bilateral feedback methods. Third, the experiments were conducted in simulations that assumed minimal time delay in communication (5-10 ms) and obstacle locations were known. Both time delay and obstacle location estimation on the physical hardware would be explored in future work. We will integrate an object detecting and position estimation algorithm developed with deep learning.

## V. Conclusion

In this work, we explore various shared-control methods with bilateral feedback through whole-body telelocomotion on a humanoid robot for obstacle avoidance in diverse environments. A time-derivative Sigmoid function (TDSF) is utilized to generate force feedback more intuitively. Extensive experiments encompassing four feedback cases and five different maps were conducted using a humanoid robot SATYRR, an HMI, and a VR headset. The experiment results indicate that when the environments are familiar to the operator, bilateral feedback often becomes a disturbance and introduces uncertainty to the control. However, bilateral feedback improves performance and is preferred when the environments are unfamiliar to the operator. In summary, our work shows the strengths and weaknesses of different bilateral feedback shared-control methods under various obstacle environments for whole-body telelocomotion of a humanoid robot. This illustrates the situational utility of different bilateral feedback shared-control methods.

## Acknowledgment

The authors are grateful to Seung Woo (William) Ok for his support in managing the experiment for the letter.

## References

[1] A. Purushottam, Y. Jung, K. Murphy, D. Baek, and J. Ramos, "Hands-free telelocomotion of a wheeled humanoid," in *Proc. IEEE/RSJ Int. Conf. Intell. Robots Syst.*, 2022, pp. 8313–8320.

[2] J. Ramos and S. Kim, "Dynamic locomotion synchronization of bipedal robot and human operator via bilateral feedback teleoperation," *Sci. Robot.*, vol. 4, no. 35, 2019, Art. no. eaav4282.

[3] J. Ramos and S. Kim, "Humanoid dynamic synchronization through whole-body bilateral feedback teleoperation," *IEEE Trans. Robot.*, vol. 34, no. 4, pp. 953–965, Aug. 2018.

[4] F. Abi-Farrajl, B. Henze, A. Werner, M. Panzirsch, C. Ott, and M. A. Roa, "Humanoid teleoperation using task-relevant haptic feedback," in *Proc. IEEE/RSJ Int. Conf. Intell. Robots Syst.*, 2018, pp. 5010–5017.

[5] M. Hwang et al., "Flexible endoscopic surgery robot system, K-FLEX," in *Proc. 18th Int. Conf. Control, Automat. Syst.*, 2018, pp. 17–20.

[6] A. Gottardi, S. Tortora, E. Tosello, and E. Menegatti, "Shared control in robot teleoperation with improved potential fields," *IEEE Trans. Hum.-Mach. Syst.*, vol. 52, no. 3, pp. 410–422, Jun. 2022.

[7] S. Luo, M. Cheng, R. Ding, F. Wang, B. Xu, and B. Chen, "Human–robot shared control based on locally weighted intent prediction for a teleoperated hydraulic manipulator system," *IEEE/ASME Trans. Mechatron.*, vol. 27, no. 6, pp. 4462–4474, Dec. 2022.

[8] S. Wang and J. Ramos, "Dynamic locomotion teleoperation of a reduced model of a wheeled humanoid robot using a whole-body human-machine interface," *IEEE Robot. Automat. Lett.*, vol. 7, no. 2, pp. 1872–1879, Apr. 2022.

[9] D. A. Abbink, M. Mulder, and E. R. Boer, "Haptic shared control: Smoothly shifting control authority?," *Cogn., Technol. Work*, vol. 14, no. 1, pp. 19–28, 2012.

[10] S. Udupa, V. R. Kamat, and C. C. Menassa, "Shared autonomy in assistive mobile robots: A review," *Disabil. Rehabil., Assistive Technol.*, vol. 18, pp. 827–848, 2023.

[11] D. P. Losey, C. G. McDonald, E. Battaglia, and M. K. O'Malley, "A review of intent detection, arbitration, and communication aspects of shared control for physical human–robot interaction," *Appl. Mechanics Rev.*, vol. 70, no. 1, 2018, Art. no. 010804.

[12] H. Wang and X. P. Liu, "Adaptive shared control for a novel mobile assistive robot," *IEEE/ASME Trans. Mechatron.*, vol. 19, no. 6, pp. 1725–1736, Dec. 2014.

[13] K.-T. Song, S.-Y. Jiang, and M.-H. Lin, "Interactive teleoperation of a mobile manipulator using a shared-control approach," *IEEE Trans. Hum.-Mach. Syst.*, vol. 46, no. 6, pp. 834–845, Dec. 2016.

[14] J. Bütepage and D. Kragic, "Human-robot collaboration: From psychology to social robotics," 2017, *arXiv:1705.10146*.

[15] J. Luo, Z. Lin, Y. Li, and C. Yang, "A teleoperation framework for mobile robots based on shared control," *IEEE Robot. Automat. Lett.*, vol. 5, no. 2, pp. 377–384, Apr. 2020.

[16] M. Selvaggio, P. R. Giordano, F. Ficuciello, and B. Siciliano, "Passive task-prioritized shared-control teleoperation with haptic guidance," in *Proc. Int. Conf. Robot. Automat.*, 2019, pp. 430–436.

[17] F. Abi-Farraj, T. Osa, N. P. J. Peters, G. Neumann, and P. R. Giordano, "A learning-based shared control architecture for interactive task execution," in *Proc. IEEE Int. Conf. Robot. Automat.*, 2017, pp. 329–335.

[18] K. Huang et al., "Telelocomotion—Remotely operated legged robots," *Appl. Sci.*, vol. 11, no. 1, 2020, Art. no. 194.

[19] O. Khatib, "Real-time obstacle avoidance for manipulators and mobile robots," in *Proc. IEEE Int. Conf. Robot. Automat.*, 1985, pp. 500–505.

[20] S. G. Hart and L. E. Staveland, "Development of NASA-TLX (Task load index): Results of empirical and theoretical research," in *Adv. Psychol.*, vol. 52, pp. 139–183, 1988.